On the Actuation Modes of a Multiloop Mechanism for Space Applications

Chuanyang Li, Jorge Angeles, *Life Fellow, IEEE*, Hongwei Guo, Dewei Tang, Rongqiang Liu, Zhongbao Qin, and Hong Xiao

***Abstract*—A symmetric, double-tripod multiloop mechanism (DTMLM), intended for grabbing objects in outerspace, is the subject of this article. Actuation modes are analyzed while introducing a novel tool applicable to space mechanisms. The key issue here lies in establishing the criteria for selecting the optimum mode from multiple actuation possibilities. The evaluation procedure includes generalized-force values, power requirement, and actuation-strategy models, along with their optimization. Accordingly, the optimization procedure targets the mode(s) with 1) uniformity of generalized-force distribution, 2) uniformity of power-requirement distribution, and 3) the fewest working actuators in a given maneuver. In this way, a rather complex problem is formulated in a simple manner, whereby the optimum actuation mode is found by list-lookup, from a reduced number of candidates. The DTMLM, which carries three compound hinges plus three prismatic, and six revolute joints, has three degrees of freedom. To analyze the actuation modes of the mechanism, the dynamics model of the DTMLM is established; as well, five representative modes are selected from 84 possibilities. It turns out that the 3R-type (three revolute actuators) shows a uniform power-requirement distribution among the three actuators in the bending motion mode; in the 3P-type (three prismatic actuators), one single actuator is operational, and hence, takes all the load. Thus, the 3R-type is the best from the power-distribution viewpoint, thereby providing strong power support, but complex from the actuation-strategy viewpoint, as illustrated in the article. Simulation results and prototype experiments of the DTMLM are reported, thereby verifying the analysis results.**

***Index Terms*—Actuation mode, double-tripod, dynamics model, evaluation criteria, multiloop mechanism.**

Manuscript received 30 July 2021; revised 14 September 2021; accepted 12 October 2021. Date of publication 30 November 2021; date of current version 17 October 2022. Recommended by Technical Editor Z. Bi. and Senior Editor W.J. Chris Zhang. This work was supported in part by the National Natural Science Foundation of China under Grant U1613201 and Grant 52005124, in part by the Youth Fund of PLA Rocket Force University of Engineering under Grant 2021QN-B023 and in part by the Youth Fund of the Natural Science Foundation of Shaanxi under Grant 2022JQ-316. The work of Jorge Angeles was supported by NSERC Canada's Natural Sciences and Engineering Research Council under Grant 4532-2010. *(Corresponding authors: Hongwei Guo; Dewei Tang.)*

Chuanyang Li and Zhongbao Qin are with the Department of Basic, PLA Rocket Force University of Engineering, Xi'an 710025, China (e-mail: li_chuanyang@yeah.net; zhongb_qin@163.com).

Hongwei Guo, Dewei Tang, Rongqiang Liu, and Hong Xiao are with the State Key Laboratory of Robotics and Systems, Harbin Institute of Technology, Harbin 150001, China (e-mail: guohw@hit.edu.cn; dwtang@hit.edu.cn; liurq@hit.edu.cn; xiaohong@hit.edu.cn).

Jorge Angeles is with the Department of Mechanical Engineering and Centre for Intelligent Machines, McGill University, Montreal, QC H3A 0C3, Canada (e-mail: angeles@cim.mcgill.ca).

Color versions of one or more figures in this article are available at https://doi.org/10.1109/TMECH.2021.3121723.

Digital Object Identifier 10.1109/TMECH.2021.3121723

I. Introduction

To implement space manipulation tasks, such as noncooperative target-tracking-and-capturing, multiloop mechanisms offer high mobility, high stiffness, high load-carrying capacity, large workspace, and high adaptability. Li *et al.* [1] proposed a novel multiloop mechanism for space applications, dubbed the double-tripod multiloop mechanism (DTMLM). The base platform (BP) of the mechanism is attached to a space vessel, while the moving platform (MP) is free. The geometry and typical postures of the DTMLM have been defined, as shown in Fig. 1. The DTMLM has two basic motion modes, namely, 1) folding and 2) bending. The process under which the DTMLM folds completely, as in Fig. 1(b), from its reference posture in Fig. 1(a) is mode (1). As well, mode (2) represents the process under which the DTMLM reaches its largest bending angle, at over 100°, in Fig. 1(c). Other maneuvers are possible as combinations of these two basic motion modes.

When a set of N modules of this kind are assembled, an N-stage manipulator is produced for capturing, as shown in Fig. 2. It is found that bending is the maneuver of interest when the manipulator is under either a grabbing task or a reconfiguration task of each DTMLM module. As well, the manipulator is folded when not in operation, for space-saving and damage-prevention [1]. Therefore, only two maneuvers of the DTMLM module, i.e., folding and bending, are considered in this article.

The DTMLM module has three degrees of freedom (dof) [2], the dof of an N-module manipulator thus being $3N$. Although the robot appears suitable for space applications, as noted above, the actuation system of such a highly redundant manipulator is complex. Therefore, the actuation-mode analysis of the whole system, as well as that of each module, becomes essential. The actuation modes of the DTMLM are analyzed in this article.

Three actuation schemes are considered: under-, full-, and redundant actuation, depending on both the mechanism dof and its number of actuators. Underactuation [3]–[5] reduces the number of actuators, weight, and complexity of a robot. However, this mode cannot provide enough mobility and stability, thereby being unsuitable for aerospace mechanisms. Redundant

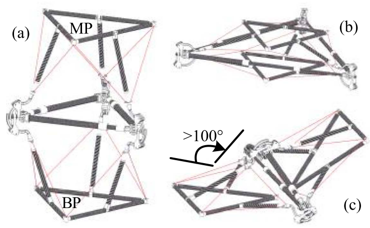

Fig. 1. Postures of the DTMLM. (a) Reference posture. (b) Folded posture. (c) Bent posture.

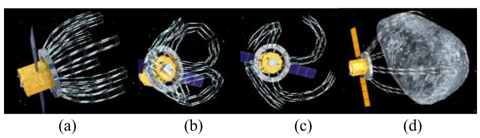

Fig. 2. Space capturing based on the DTMLM manipulator. (a) Eight-finger version. (b) Reconfiguration task. (c) Four-finger version. (d) Capture tasks targeting space bodies.

actuation, generally, is employed for singularity avoidance [6], [7] and high payload capacity [8], at the expense of system simplicity. However, most singularity postures of the DTMLM occur on the boundary of its workspace [1], full actuation thus being the choice in light of its functionality and stability.

This article was motivated by the need to actuate an N-module DTMLM manipulator, intended for grabbing operations in outer space. Such applications have special features, because a space-borne mechanism brings about issues at the design stage that are not found in the same kind of mechanisms mounted on a fixed (to the Earth) base. In the latter, it is apparent that the actuators should be located on the BP, just to reduce the inertial load on the actuators. In the case of space-borne mechanisms, however, the number of possibilities on where to locate the actuators is much richer. While these mechanisms offer many possibilities for the location of the actuators, they also pose interesting problems, not present in their fixed-based counterparts.

With reference only to the floating mechanisms of interest, the rich number of actuation possibilities calls for an optimum solution. That is, the choice of actuation mode has to be formulated as an optimization problem.

In the realm of actuation optimization, numerous contributions have been reported. Actuator torque-distribution methods have been studied for: i) minimization of the peak value of the required actuator torque [9]; ii) inverse-dynamics analyses [10], [11]; iii) global kinetic-energy minimization [12]; iv) optimization of the driving forces [13]; v) high-regeneration efficiency [14]; and vi) reduction in energy consumption [15]. As well, actuator energy consumption has been optimized for multiobjective path-placement optimization [16] and energy-saving [17]–[20]. Other applications target actuator-force optimization for reduction of overall cost and size of the actuators [21]. However, all these studies, to the authors' knowledge, focus on given actuation systems, and, hence, are not suitable for our application, i.e., finding the optimum selection of actuation mode(s) in the design process.

Furthermore, Wang *et al.* [22] proposed a general formulation of the optimization problem for the placement and sizing of piezoelectric actuators in feedforward control systems. Mu *et al.* [23] explored the influence of the location and the number of actuators on the modal force of a rectangular plate, thereby enhancing actuation capability while alleviating stress concentrations. Wang *et al.*'s and Mu *et al.*'s works both addressed the location of the actuators in the target system, one focusing on piezoelectric actuators, and the other on the actuation of the plate. These solutions are thus unsuitable for rigid actuators like electric motors, and aerospace mechanisms, such as those in the DTMLM. Shin and Kim [24] proposed a distributed actuation method for designing a finger-type manipulator with a sliding-actuation mechanism. This method has advantages on force optimization and structure miniaturization. However, the method is not applicable in the presence of revolute actuators. For this reason, this method cannot be employed in the DTMLM. Nieto *et al.* [25] applied convex optimization with minimization of energy consumption and peak power. Lagger *et al.* [26] resorted to a power-distribution unit comprising a motor-cum-differential-gear transmission, to provide mechanical torque to one of the electromechanical actuators. The foregoing works offer solutions in actuation-system design, but cannot be applicable to the selection of the optimum actuation mode(s) in the case of the the DTMLM. Zhao *et al.* [27] analyzed the relationship between the workspace of a metamorphic serial-parallel manipulator and different actuator-distribution layouts. However, the presence of different actuation modes of the manipulator requires the adjustment of metamorphic joints. The actuation-distribution analysis being valid only for one specific system, it cannot lead to a general optimization strategy. Ding and his co-workers [28], [29] proposed a method for the optimal design of space deployable mechanisms, but this procedure cannot be employed in the optimal design of actuation systems. New evaluation criteria for the optimization of actuation modes of the DTMLM should thus be explored.

In this article, an actuation-mode evaluation procedure is proposed, based on three criteria: i) generalized-force distribution; ii) power-requirement distribution; and iii) actuation strategy. Since we consider only two types of actuators, prismatic ($\mathtt{P}$) or revolute ($\mathtt{R}$), in addition to the location of the actuators, the criteria of interest lead to different viewpoints on the optimum selection of the actuation mode. Accordingly, a rather complex problem, i.e., selecting the optimum actuation mode from multiple actuation possibilities, is formulated in a simple manner by means of a pertinent evaluation procedure. This leads to a simple choice among the elements of a discrete, reduced set.

II. Description of the DTMLM

The DTMLM [1], whose kinematic chain is shown in Fig. 3(a), carries nine revolute, six spherical, and three prismatic joints. Two spherical joints and one revolute joint constitute one coupled *cell*, the concept of cell in mechanisms defined in an earlier paper [30]. An example of a cell is the SRS *assembly*,

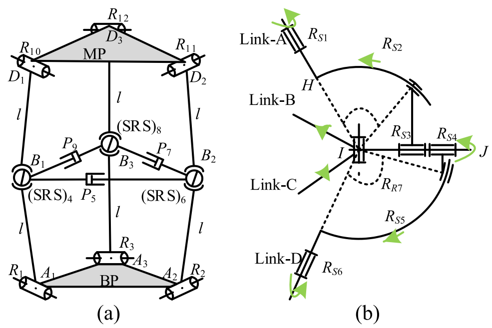

Fig. 3. DTMLM. (a) Architecture. (b) Schematic of the SRS chain.

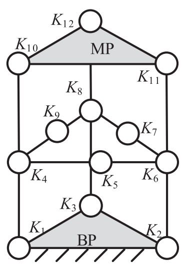

Fig. 4. DTMLM in cell methodology.

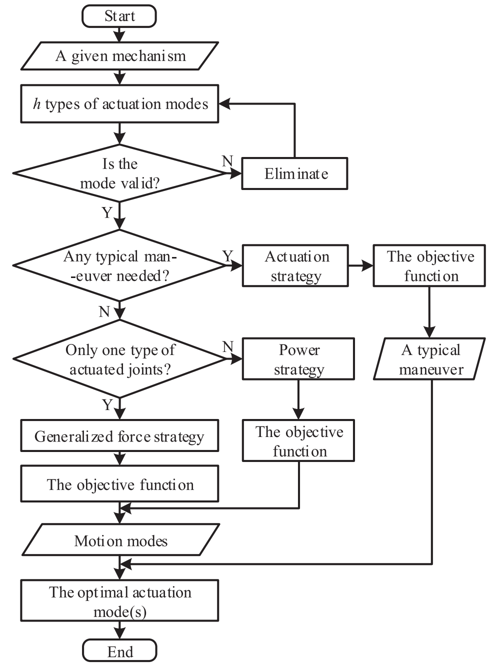

Fig. 5. Procedure for the selection of the optimum actuation mode.

whose kinematic chain is depicted in Fig. 3(b). Both R_{S2} and R_{S5} consist of a curved rail and a curved groove. The equivalent axis of R_{S2} is perpendicular to the HIJ plane and passes through point I when the curved rail slides along the curved groove. Thus, R_{S2} (R_{S5}) is an equivalent revolute joint.

The mechanism carries one BP and one MP, which are represented by identical equilateral triangles in Fig. 3. The two platforms and the middle plane $B_1B_2B_3$, referred to as the "mid plane," are connected by links A_iB_i and B_iD_i, for $i = 1, 2, 3$. All six links carry the same length, henceforth denoted l. Thus, the two platforms are symmetrically located with respect to the mid-plane.

The mobility and singularity analyses of the mechanism are conducted based on the concept of cell methodology (CM) [2]. The pertinent CM model is shown in Fig. 4, where $K_1 \ldots K_{12}$ are *cells* of the mechanism. K_1, K_2, K_3, K_{10}, K_{11}, and K_{12} denote the revolute joints; K_4, K_6, and K_8 denote, each, a SRS subchain, which is a composite cell; K_5, K_7, and K_9 denote prismatic joints.

III. Actuation-Mode Evaluation

Actuation mode is a concept pertaining to the driving of a given mechanism. We distinguish between *homogeneous* and *inhomogeneous* modes. In the former, the actuators are of the same type, either R or P. An inhomogeneous mode involves actuators of both types.

The actuation-mode evaluation of the subsystems of a *given mechanism* is the subject of this section. First and foremost, given that the dof of the system under development has been already determined, namely, n, the issues to be discussed are 1) the type of single-dof actuator, either R or P, to be used, and 2) the placement of each actuator, which can be any single-dof joint of the whole system. Evaluation criteria for the alternatives are also introduced.

A. Evaluation Procedure and Three Evaluation Criteria

The *evaluation procedure* is intended to guide the designer into the optimum selection of the actuation mode(s).

At the outset, all possibilities of the actuator type are considered. Given that n actuators are at play, and each can be of any of the two foregoing types, the total number of possible alternatives amounts to

$$h = C_m^n = \frac{m \times (m-1) \times \cdots \times (m-n+1)}{n!} \qquad (1)$$

where m denotes the total number of one-dof lower kinematic pairs (LKPs) in the mechanism.

Moreover, a *test maneuver* is assumed, that describes thoroughly the manipulation requirements from the given mechanism, henceforth referred to as *the system*.

Three evaluation criteria are established at the outset: 1) *uniformity of generalized-force distribution*; 2) *uniformity of power distribution*; and 3) *actuation-strategy criterion*.

As per the procedure shown in Fig. 5, the criteria involve different viewpoints that consider paradigm application cases. In this way, criterion i) is applied when only one type of homogeneous submode (R or P) is used in the given mechanism, while criterion ii) is the choice when a) two types of homogeneous submodes are applied, and b) the inhomogeneous submode is involved. When the main tasks of the given mechanism are considered for a particular test maneuver, case iii) applies. The details of the three criteria are included below.

B. Uniformity of Generalized-Force Distribution

a) Actuator Generalized Force: The actuator generalized force is derived from the dynamics model of the given mechanism. Then, the generalized-force array is

$$\mathbf{f}_k = \begin{bmatrix} \phi_{k,1} & \phi_{k,2} & \cdots & \phi_{k,s} & \phi_{k,s+1} & \cdots & \phi_{k,n} \end{bmatrix}^T$$
$$k = 1, 2, \ldots, h, \quad s = 1, 2, \ldots, n \tag{2}$$

where $\mathbf{f}_k$ is the actuated-torque array of the kth mode in the case in which all LKPs are R joints, while the actuated-force array when all LKPs are P joints.

b) Evaluation Criterion: In general, it is expected to achieve an even distribution of the actuator generalized forces, the actuation mode with the most even distribution being our objective. In this case, the *variance* of the actuator generalized forces of each actuation mode is applied to represent the indicator of its distribution evenness, while κ, the order number of the kth actuation mode, turns out to be the single variable. Thus, the objective function for this criterion is formulated as

$$\min_{\kappa} F_k = F_k(\kappa), \quad \kappa \in [1, h] \tag{3}$$

with

$$F_k = \frac{\sum_{s=1}^{n} (\phi_{k,s} - \bar{\phi}_k)^2}{n}, \quad \bar{\phi}_k = \frac{\sum_{s=1}^{n} \phi_{k,s}}{n} \tag{4}$$

$\bar{\phi}_k$ thus denoting the mean value of the actuator generalized forces.

Then, the variance of the optimum actuation mode is

$$F = \min\{F_1, F_2, \ldots, F_k, \ldots, F_h\}. \tag{5}$$

Once the variances of the actuator generalized force of the h actuation modes are obtained, the optimum mode is found from (5) by simple *list-lookup*, a simple version of *table-lookup*.

C. Uniformity of Power Distribution

The power required to drive the mechanism through a certain task is applicable to both homogeneous and inhomogeneous actuation modes.

Under the assumption that the actuator system includes r revolute and p prismatic pairs, we have

$$\mathbf{w} = \begin{bmatrix} \mathbf{w}_r \\ \mathbf{w}_p \end{bmatrix} = [\underbrace{\tau_1, \ldots, \tau_i, \ldots, \tau_r}_{\mathbf{w}_r^T}, \underbrace{f_1, \ldots, f_j, \ldots, f_p}_{\mathbf{w}_p^T}]^T \tag{6}$$

with $\mathbf{w}$ denoting the generalized-force array, τ_i the driving torque of the ith actuated revolute joint, and f_j the driving force of the jth actuated prismatic joint.

A subscript k is introduced to denote the kth actuation mode out of h possibilities. Then, the generalized-force array of the kth actuation mode is

$$\mathbf{w}_k = [\underbrace{\tau_{k,1}, \ldots, \tau_{k,i}, \ldots, \tau_{k,r}}_{\mathbf{w}_{r,k}^T}, \underbrace{f_{k,1}, \ldots, f_{k,j}, \ldots, f_{k,p}}_{\mathbf{w}_{p,k}^T}]^T. \tag{7}$$

The power requirement Q_s, from the sth $(s = 1, 2, \ldots, n)$ actuator, is the *product* of the generalized force times the generalized velocity. In this article, we set $P_s = |Q_s|$ to simplify the criterion representation. Thus, the power-requirement array of the kth $(k = 1, 2, \ldots, h)$ actuation mode is

$$\mathbf{p}_k = \begin{bmatrix} P_{k,1} & P_{k,2} & \cdots & P_{k,s} & \cdots & P_{k,n} \end{bmatrix}^T$$
$$= \begin{bmatrix} |\tau_{k,1}\dot{\theta}_{k,1}| & \cdots & |\tau_{k,r}\dot{\theta}_{k,r}| & |f_{k,1}\dot{c}_{k,1}| & \cdots & |f_{k,p}\dot{c}_{k,p}| \end{bmatrix}^T. \tag{8}$$

A test maneuver should ideally require an even distribution of the power requirement among all the actuators, R or P. Accordingly, the variance of the power requirement of each actuation mode is an indicator of its distribution evenness, seen as a function of κ. Hence, the objective function, in this case, is

$$\min_{\kappa} D_k = D_k(\kappa), \quad \kappa \in [1, h] \tag{9}$$

with

$$D_k = \frac{\sum_{s=1}^{n} (P_{k,s} - \bar{P}_k)^2}{n}, \quad \bar{P}_k = \frac{\sum_{s=1}^{n} P_{k,s}}{n}. \tag{10}$$

Then, the power-requirement variance of the optimum actuation mode is

$$D = \min\{D_1, D_2, \ldots, D_k, \ldots, D_h\}. \tag{11}$$

Thus, the optimum mode is obtained from (11) by simple list-lookup.

D. Actuation-Strategy Criterion

Different criteria will lead to different optimum solutions. The *actuation-strategy criterion* is a measure of the simplicity of the actuation strategy of a test maneuver. For this criterion, accordingly, the fewer *the actuators needed for the maneuver*, the simpler the actuation strategy. Thus, the objective function of this case turns out to be

$$\min_{\kappa} M_k = M_k(\kappa), \quad \kappa \in [1, h] \tag{12}$$

where M_k $(k = 1, 2, \ldots, h)$, derived from the kinematics analysis, denotes the number of actuators needed by the kth actuation mode for the prescribed test maneuver.

Therefore, the optimum actuation mode is selected from

$$M = \min\{M_1, M_2, \ldots, M_k, \ldots, M_h\}, \quad M_k \le n. \tag{13}$$

IV. Dynamics Model of the DTMLM

The DTMLM includes both R and P actuated joints, criterion (ii) thus being employed. The dynamics model of the DTMLM is established in this section.

The DTMLM consists of 14 links, i.e., one BP and 13 moving rigid bodies, as per Fig. 3, with the center of mass (c.o.m.)[1] of the jth $(j = 1, 2, \ldots, 13)$ link, labeled C_j in Fig. 6. The mechanism has three dof [2]; we thus assume that a 3R actuation mode is

[1]Unless otherwise indicated, we assume that all mechanism bars are slender rods, of uniform cross sections, and their centers of mass thus lying in their middle.

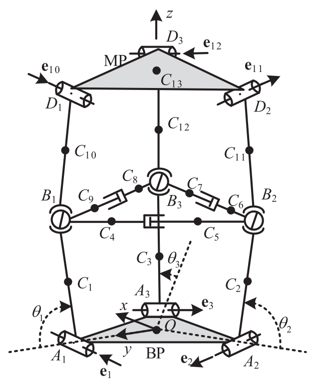

Fig. 6. Differential kinematics model of the DTMLM.

applied in this model, all twists of the 13 moving rigid bodies being represented in terms of actuated-joint rates $\dot{\theta}_i$, for $i = 1, 2, 3$, and the corresponding angles being shown in Fig. 6.

The twists of the moving rigid bodies are referred to as $\mathbf{t}_j = \sum_{i=1}^{3} \dot{\theta}_i \mathbf{t}_{ji}$, with $\mathbf{t}_{ji}$ denoting the motion of the jth link with respect to the ith actuated joint. All $\mathbf{t}_{ji}$ terms are given in the Appendix. Thus, the array $\mathbf{t}$ of system twist can be expressed as

$$\mathbf{t} = \mathbf{T}\dot{\mathbf{q}} \tag{14}$$

in which

$$\mathbf{t} = \begin{bmatrix} \mathbf{t}_1 \\ \mathbf{t}_2 \\ \mathbf{t}_3 \\ \mathbf{t}_4 \\ \vdots \\ \mathbf{t}_{13} \end{bmatrix}, \quad \mathbf{T} = \begin{bmatrix} \mathbf{t}_{11} & \mathbf{0} & \mathbf{0} \\ \mathbf{0} & \mathbf{t}_{22} & \mathbf{0} \\ \mathbf{0} & \mathbf{0} & \mathbf{t}_{33} \\ \mathbf{t}_{41} & \mathbf{t}_{42} & \mathbf{t}_{43} \\ \vdots & \vdots & \vdots \\ \mathbf{t}_{13,1} & \mathbf{t}_{13,2} & \mathbf{t}_{13,3} \end{bmatrix}, \quad \dot{\mathbf{q}} = \begin{bmatrix} \dot{\theta}_1 \\ \dot{\theta}_2 \\ \dot{\theta}_3 \end{bmatrix} \tag{15}$$

where $\mathbf{0}$ denotes the six-dimensional zero vector, $\mathbf{T} \in \mathbf{R}^{78\times 3}$ being the *twist shaping matrix* of the DTMLM.

Then, the Newton–Euler equation of the jth link is

$$\mathbf{M}_j \dot{\mathbf{t}}_j = -\mathbf{W}_j \mathbf{M}_j \mathbf{t}_j + \mathbf{w}_j^A + \mathbf{w}_j^D + \mathbf{w}_j^C + \mathbf{w}_j^G \tag{16}$$

in which

$$\mathbf{M}_j = \begin{bmatrix} \mathbf{I}_j & \mathbf{O}_{3\times 3} \\ \mathbf{O}_{3\times 3} & m_j \mathbf{1}_{3\times 3} \end{bmatrix}, \quad \mathbf{W}_j = \begin{bmatrix} \mathbf{\Omega}_j & \mathbf{O}_{3\times 3} \\ \mathbf{O}_{3\times 3} & \mathbf{O}_{3\times 3} \end{bmatrix}$$

$$\mathbf{w}_j^G = \begin{bmatrix} \mathbf{0} \\ m_j \mathbf{g} \end{bmatrix} \tag{17}$$

where $\mathbf{M}_j$ denotes the 6×6 inertia dyad of the jth link, $\mathbf{W}_j$ the 6×6 angular-velocity dyad of the same body; $\mathbf{w}_j^A$, $\mathbf{w}_j^D$, $\mathbf{w}_j^G$, and $\mathbf{w}_j^C$ represent the wrenches generated by active, dissipative, gravity, and non-working constraint forces and moments, respectively; and $\mathbf{I}_j \in \mathbf{R}^{3\times 3}$, m_j, and $\mathbf{\Omega}_j \in \mathbf{R}^{3\times 3}$ represent the inertia tensor at the c.o.m, the mass, and the cross-product matrix of $\boldsymbol{\omega}_j$ of the jth link, respectively.

Combining the foregoing terms of all the links, the dynamics model of the DTMLM is described by a 78-uncoupled model, namely,

$$\mathbf{M}\dot{\mathbf{t}} = -\mathbf{W}\mathbf{M}\mathbf{t} + \mathbf{w}^A + \mathbf{w}^D + \mathbf{w}^C + \mathbf{w}^G \tag{18}$$

in which

$$\mathbf{M} = \mathrm{diag}(\mathbf{M}_1, \ldots, \mathbf{M}_{13}), \quad \mathbf{W} = \mathrm{diag}(\mathbf{W}_1, \ldots, \mathbf{W}_{13})$$

$$\mathbf{w}^A = \begin{bmatrix} \mathbf{w}_1^A \\ \vdots \\ \mathbf{w}_{13}^A \end{bmatrix}, \mathbf{w}^D = \begin{bmatrix} \mathbf{w}_1^D \\ \vdots \\ \mathbf{w}_{13}^D \end{bmatrix}, \mathbf{w}^C = \begin{bmatrix} \mathbf{w}_1^C \\ \vdots \\ \mathbf{w}_{13}^C \end{bmatrix}, \mathbf{w}^G = \begin{bmatrix} \mathbf{w}_1^G \\ \vdots \\ \mathbf{w}_{13}^G \end{bmatrix} \tag{19}$$

Thus,

$$\mathbf{I}(\mathbf{q})\ddot{\mathbf{q}} = -\mathbf{C}(\mathbf{q}, \dot{\mathbf{q}})\dot{\mathbf{q}} + \boldsymbol{\tau} + \boldsymbol{\delta} + \boldsymbol{\gamma} \tag{20}$$

in which

$$\mathbf{I}(\mathbf{q}) = \mathbf{T}^T \mathbf{M}\mathbf{T} \in \mathbf{R}^{3\times 3}$$
$$\mathbf{C}(\mathbf{q}, \dot{\mathbf{q}}) = \mathbf{T}^T \mathbf{M}\dot{\mathbf{T}} + \mathbf{T}^T \mathbf{W}\mathbf{M}\mathbf{T} \in \mathbf{R}^{3\times 3}$$
$$\boldsymbol{\tau} = \mathbf{T}^T \mathbf{w}^A, \boldsymbol{\delta} = \mathbf{T}^T \mathbf{w}^D, \boldsymbol{\gamma} = \mathbf{T}^T \mathbf{w}^G \tag{21}$$

where $\boldsymbol{\tau}$, $\boldsymbol{\delta}$, and $\boldsymbol{\gamma}$ denote the generalized actuated-, dissipative-, and gravity-force arrays, respectively.

TABLE I
ACTUATION MODES

Type	Mode			
3R	$\boldsymbol{K_1K_2K_3}$	$K_1K_2K_{12}$	$K_1K_{11}K_{12}$	$K_{10}K_{11}K_{12}$
2R1P	$\boldsymbol{K_1K_3K_5}$	$K_1K_5K_{12}$	$K_3K_5K_{10}$	$K_5K_{11}K_{12}$
1R2P	$\boldsymbol{K_1K_5K_7}$	$\boldsymbol{K_2K_5K_7}$	$K_5K_7K_{10}$	$K_5K_7K_{11}$
3P	$\boldsymbol{K_5K_7K_9}$			

V. ACTUATION-MODE ANALYSIS OF THE DTMLM

A. Potential Actuation Modes

As mentioned earlier, the DTMLM has three dof, and hence, it needs three actuators. As shown in Figs. 3 and 4, $K_1 \ldots K_3$ and $K_{10} \ldots K_{12}$ denote the revolute joints; K_5, K_7, and K_9 denote, in turn, the prismatic joints. The nine foregoing joints are single LKPs, three of them actuated. By virtue of the gravity-free environment, 84 actuator possibilities are available.

However, two kinds of modes are unsuitable for driving the mechanism, which occur when a) for the 3R-type, two R actuators are symmetrically located with respect to the mid-plane; and b) for the 2R1P-type, one P actuator directly connects two links with R actuators. For example, the R actuators K_1 and K_{10} of the $K_1K_2K_{10}$ mode work symmetrically and synchronously, since the mechanism undergoes a symmetric motion with respect to the mid-plane. Accordingly, K_1 and K_{10} work as one single R actuator under any posture, the mode thus being underactuated. As well, in mode $K_1K_2K_5$, a two-dof loop $K_1K_2K_6K_5K_4$ is driven by three actuators, the mechanism thus being underactuated. Therefore, these two kinds of actuation modes can control only two dof. These cases are thus eliminated.

Hence, only 51 of the 84 modes are feasible. As shown in Table I, 13 modes are obtained by means of the symmetry of the mechanism.

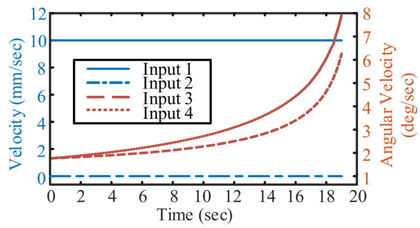

Fig. 7. Actuator input signals.

TABLE II
INPUTS OF THE ACTUATION MODES

Mode	$K_1K_2K_3$			$K_1K_3K_5$			$K_1K_5K_7$		
Actuator	K_1	K_2	K_3	K_1	K_3	K_5	K_1	K_5	K_7
Folding	3	3	3	3	3	1	3	1	1
Bending	3	3	4	3	4	1	3	1	2
Mode	$K_2K_5K_7$			$K_5K_7K_9$					
Actuator	K_2	K_5	K_7	K_5	K_7	K_9			
Folding	3	1	1	1	1	1			
Bending	3	1	2	1	2	2			

B. Given Maneuvers Based on Bending and Folding Motion Modes

All actuation modes operate under the following conditions: 1) A mechanism posture, to be attained by any actuation mode, is prescribed; 2) the prescribed mechanism trajectory, i.e., the time-histories of *all* the joints, is the same for all modes; 3) the twist history of the MP is the same for all modes; 4) the mechanism achieves the prescribed bent and folded posture; and 5) the load on the MP is the same for all actuation modes.

At one instant, the total power requirement from the three actuators, for different modes, is the same for a given maneuver. However, the power-requirement distribution among the three actuators varies for different actuation modes. To simplify the analysis process, five of the 13 actuation modes shown in Table I are analyzed in this article: $K_1K_2K_3$(3R), $K_1K_3K_5$(2R1P), $K_1K_5K_7$(1R2P-A), $K_2K_5K_7$(1R2P-B), and $K_5K_7K_9$(3P). In the case of power-requirement distribution, we impose the criterion that the optimum actuation mode is the one that leads to a *uniform* power requirement among all actuators, as shown in (9). As well, in the actuation-strategy criterion, the optimum actuation mode is the one with the lowest number of working actuators in the folding and bending motion modes, as shown in (12).

The folding and bending maneuvers are implemented by all actuation modes, 3R, 3P, 2R1P, and 1R2P. Four input signals are given in Fig. 7. Three of them are combined in light of various actuation modes, as shown in Table II, where i $(i = 1, \ldots, 4)$ denotes the ith input signal in Fig. 7.

C. Power-Requirement Distribution Criterion

1) Twist Arrays:

i) For the $K_1K_2K_3$ mode, the twist array of the mechanism being that in (14), set $\dot{\mathbf{q}}_1 = \mathbf{Q}_1\dot{\mathbf{q}}$: $\dot{\mathbf{q}}_1 = [\dot{\theta}_1, \dot{\theta}_2, \dot{\theta}_3]^T$.

ii) For the $K_5K_7K_9$ mode, the actuated-joint array turns out to be $\dot{\mathbf{q}}_2 = [\dot{b}_{12}, \dot{b}_{23}, \dot{b}_{31}]^T$, the relation between $\dot{\mathbf{q}}$ and $\dot{\mathbf{q}}_2$ thus being

$$\dot{\mathbf{q}}_2 = \mathbf{Q}_2\dot{\mathbf{q}}$$

$$\mathbf{Q}_2 = \begin{bmatrix} (-\mathbf{e}_1 \times l\mathbf{a}_1)^T\mathbf{n}_{12} & (\mathbf{e}_2 \times l\mathbf{a}_2)^T\mathbf{n}_{12} & 0 \\ 0 & -(\mathbf{e}_2 \times l\mathbf{a}_2)^T\mathbf{n}_{23} & (\mathbf{e}_3 \times l\mathbf{a}_3)^T\mathbf{n}_{23} \\ (\mathbf{e}_1 \times l\mathbf{a}_1)^T\mathbf{n}_{31} & 0 & -(\mathbf{e}_3 \times l\mathbf{a}_3)^T\mathbf{n}_{31} \end{bmatrix}. \tag{22}$$

In any mechanism posture, all entries of $\mathbf{Q}_2$ cannot be eliminated, $\mathbf{Q}_2$ being a nonsingular matrix. The twist array of the mechanism is thus given by

$$\mathbf{t} = \mathbf{T}\mathbf{Q}_2^{-1}\dot{\mathbf{q}}_2 \tag{23}$$

similarly, the twist array of other actuation modes are.

iii) $K_1K_3K_5$ mode

$$\mathbf{t} = \mathbf{T}\mathbf{Q}_3^{-1}\dot{\mathbf{q}}_3, \quad \dot{\mathbf{q}}_3 = \begin{bmatrix} \dot{\theta}_1 & \dot{b}_{12} & \dot{\theta}_3 \end{bmatrix}^T \tag{24a}$$

and

$$\mathbf{Q}_3 = \begin{bmatrix} 1 & 0 & 0 \\ -(\mathbf{e}_1 \times l\mathbf{a}_1)^T\mathbf{n}_{12} & (\mathbf{e}_2 \times l\mathbf{a}_2)^T\mathbf{n}_{12} & 0 \\ 0 & 0 & 1 \end{bmatrix}. \tag{24b}$$

iv) $K_1K_5K_7$ mode

$$\mathbf{t} = \mathbf{T}\mathbf{Q}_4^{-1}\dot{\mathbf{q}}_4, \quad \dot{\mathbf{q}}_4 = \begin{bmatrix} \dot{\theta}_1 & \dot{b}_{12} & \dot{b}_{23} \end{bmatrix}^T \tag{25a}$$

and

$$\mathbf{Q}_4 = \begin{bmatrix} 1 & 0 & 0 \\ -(\mathbf{e}_1 \times l\mathbf{a}_1)^T\mathbf{n}_{12} & (\mathbf{e}_2 \times l\mathbf{a}_2)^T\mathbf{n}_{12} & 0 \\ 0 & -(\mathbf{e}_2 \times l\mathbf{a}_2)^T\mathbf{n}_{23} & (\mathbf{e}_3 \times l\mathbf{a}_3)^T\mathbf{n}_{23} \end{bmatrix}. \tag{25b}$$

v) $K_2K_5K_7$ mode

$$\mathbf{t} = \mathbf{T}\mathbf{Q}_5^{-1}\dot{\mathbf{q}}_5, \quad \dot{\mathbf{q}}_5 = \begin{bmatrix} \dot{b}_{12} & \dot{\theta}_2 & \dot{b}_{23} \end{bmatrix}^T \tag{26a}$$

and

$$\mathbf{Q}_5 = \begin{bmatrix} -(\mathbf{e}_1 \times l\mathbf{a}_1)^T\mathbf{n}_{12} & (\mathbf{e}_2 \times l\mathbf{a}_2)^T\mathbf{n}_{12} & 0 \\ 0 & 1 & 0 \\ 0 & -(\mathbf{e}_2 \times l\mathbf{a}_2)^T\mathbf{n}_{23} & (\mathbf{e}_3 \times l\mathbf{a}_3)^T\mathbf{n}_{23} \end{bmatrix}. \tag{26b}$$

2) Power Requirement:

The power consumption of the DTMLM caused by the friction forces is the same for all five actuation modes when the DTMLM undergoes the same maneuver, the dissipative forces thus having no impact on the actuation-mode optimization. As well, in the actuation-system-design process, the materials and geometry of the links are not prescribed, and thereby friction forces cannot be solved. Therefore, the dissipative-force array $\boldsymbol{\delta}$ in (20) is set as zero.

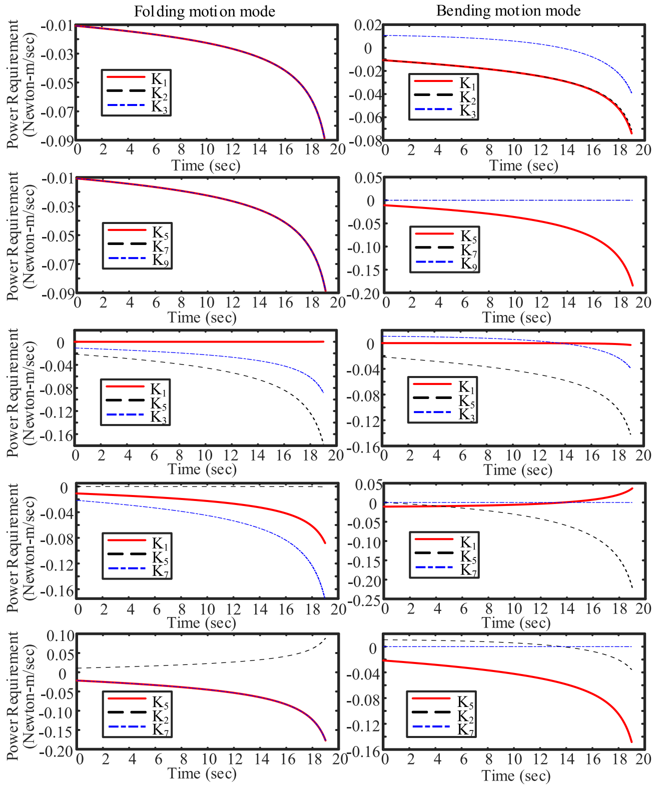

Fig. 8. Power requirements of actuators in the five actuation modes (obtained via the dynamics model).

Upon (a) (14), (b) the shaping relation in (22)–(26), and (c) inputs in Table II into the dynamics model of the DTMLM, the power requirement in the five actuation modes are calculated both under the folding and the bending modes, and then plotted in Fig. 8.

D. Actuation Strategy

When we have enough power support for each actuator, a simple actuation strategy for a specific task plays an important role. From the viewpoint of the actuation-strategy criterion in Section III-D, one single actuator, K_5, of $K_5K_7K_9$, is operational in the bending motion mode [1], and three under the modes $K_1K_2K_3$. We thus have $M_{\mathsf{3R}} = 3$, $M_{\mathsf{3P}} = 1$, $M_{\mathsf{2R1P}} = 3$, and $M_{\mathsf{1R2P}} = 2$. Clearly,

$$M_{\mathsf{3R}} = M_{\mathsf{2R1P}} > M_{\mathsf{1R2P}} = 2 > M_{\mathsf{3P}} \tag{27}$$

the 3P-type thus being the optimum solution.[2]

E. Optimum Actuation Mode(s)

According to the power-distribution criterion in Section III-C, absolute values are taken for calculating the variances. Here we have the variance of the power requirement of the five actuation modes, as shown in Fig. 9.

[2]This is meaningful for an N-module DTMLM manipulator. Within the power capacity of each actuator, only N prismatic actuators, instead of $3N$ revolute actuators, are operational for a bending maneuver, when each module carries a 3P-type actuation mode.

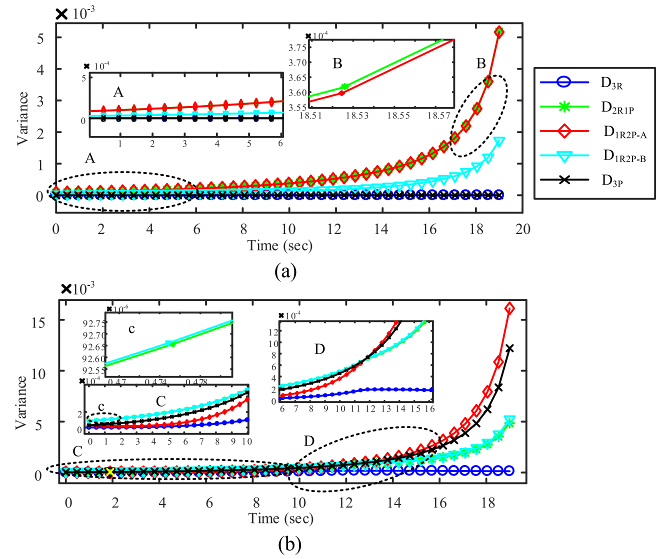

Fig. 9. Variance of power requirement. (a) Folding motion mode. (b) Bending motion mode.

TABLE III
COMPARISON AMONG THE ACTUATION MODES

Viewpoint	Maneuver	Comparison	Result	The optimum mode(s)
Power-distribution	Folding	$D_{\mathrm{2R1P}} > D_{\mathrm{1R2P-}A} > D_{\mathrm{1R2P-B}} > D_{\mathrm{3R}} \approx D_{\mathrm{3P}} \approx 0$	$D = D_{\mathrm{3R}} = D_{\mathrm{3P}}$	3R&3P
	Bending	Firstly, $D_{\mathrm{1R2P-B}} > D_{\mathrm{2R1P}} > D_{\mathrm{3P}} > D_{\mathrm{1R2P-A}} > D_{\mathrm{3R}}$, then, $D_{\mathrm{1R2P-A}} > D_{\mathrm{3P}} > D_{\mathrm{1R2P-B}} > D_{\mathrm{2R1P}} > D_{\mathrm{3R}}$	$D = D_{\mathrm{3R}}$	3R
Actuation-strategy	Folding	$M_{\mathrm{3R}} = 3,\ M_{\mathrm{2R1P}} = 3,\ M_{\mathrm{1R2P}} = 3,\ M_{\mathrm{3P}} = 3$	$M = 3$	The same
	Bending	$M_{\mathrm{3R}} = 3,\ M_{\mathrm{2R1P}} = 3,\ M_{\mathrm{1R2P}} = 2,\ M_{\mathrm{3P}} = 1$	$M = 1$	3P

The results plotted in Fig. 9 (for the power-distribution criterion) and Table II (for the actuation-strategy criterion) are summarized in Table III.

From Table III, it is apparent that the 3R-type shows a uniform power-requirement distribution among the three actuators. From the viewpoint of actuation-strategy, the 3P-type, one single actuator is operational in the bending maneuver, thus simplifying actuation and control in space-capturing applications. This mode is, therefore, the optimum.

VI. SIMULATION

An ADAMS model of the DTMLM module, as shown in Fig. 10, is described below, with all links made of aluminum, the mass of the actuators being ignored, while gravity effects are considered in the analysis, to match the case of prototype and tests on the ground.

The simulation results of 3R and 3P modes are plotted in Fig. 11. Obviously, the ADAMS plots match those in Fig. 8, which were calculated via the dynamics model. Thus, the dynamics model is verified, the actuation-mode optimal analysis in Section V-C following suit.

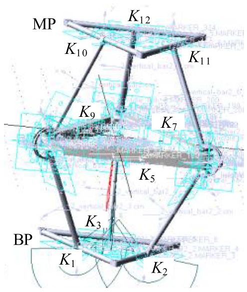

Fig. 10. ADAMS model of the DTMLM module.

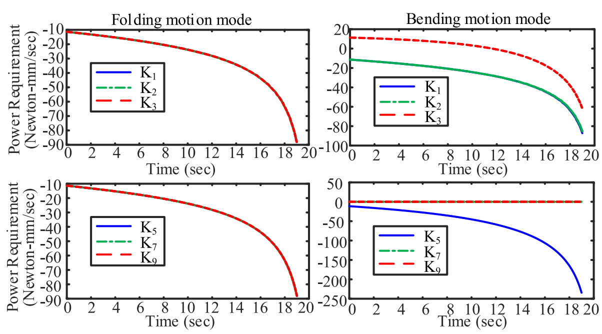

Fig. 11. Power requirements of three actuators under folding- and bending-motion modes (obtained via the ADAMS model).

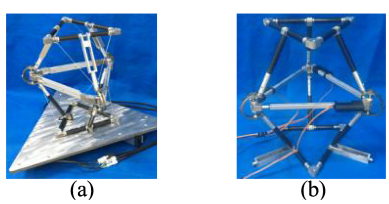

Fig. 12. Prototypes. (a) 3R-type. (b) 3P-type.

TABLE IV
PARAMETERS OF THE MANIPULATOR PROTOTYPE

Item	Parameters	Item	Parameters
Rotary actuator	MHMF022L1V2M 1800		
Translational actuator	Actuonix P16-200-256-12-P		
$\|A_1A_2\|$	240mm	l	207.84mm
$\|B_1B_2\|$	280–480mm		

VII. Prototype and Tests

A. Experimental System

3R and 3P actuation modes, the optimum solutions in the two criteria, are employed for the prototype, as shown in Fig. 12. The parameters of the prototypes are listed in Table IV. The two prototypes undergo two basic motion modes, as shown in Fig. 13.

B. Verification of the Dynamics Model

The dynamics model of the DTMLM is verified by means of the 3P prototype, under two basic motion modes.

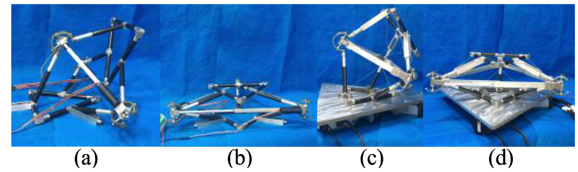

Fig. 13. Maneuvers for two prototypes. (a) 3P-bending. (b) 3P-folding. (c) 3R-bending. (d) 3R-folding.

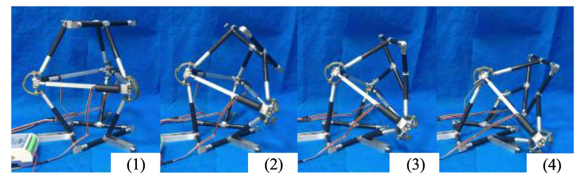

Fig. 14. Process of the bending motion mode.

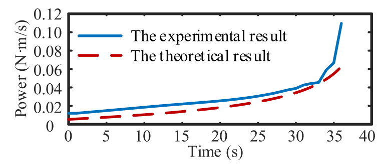

Fig. 15. Experimental and theoretical results under bending mode.

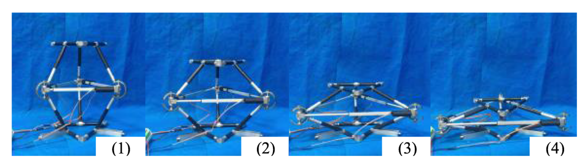

Fig. 16. Process of the folding motion mode.

1) Bending Mode: As shown in Fig. 14, one P actuator is extended from 290 to 470 mm, at a rate of about 4.8 mm/s, while the other two actuators remain passive.

Plots of theoretical and experimental results are shown in Fig. 15.

Fig. 15 shows that the power requirement follows the same trend in prototype and model, but the experimental amplitude is larger. The underlying reason is that, in the theoretical result, the motions of the SRS chains and friction are neglected.[3] Thus, the dynamics model of the DTMLM is acceptable.

2) Folding Mode: All three actuators are extended from 290 to 470 mm, under a speed of about 4.8 mm/s, to realize the folded posture, as shown in Fig. 16.

Plots of both theoretical and experimental results are shown in Fig. 17. This figure shows that the power requirement follows the same trend in both tests and model, while the experimental amplitude is larger, because the motions of the SRS chains and friction are neglected in the theoretical result. Thus, the dynamics model of the DTMLM is deemed to be acceptable. Therefore, the actuation-mode optimization under the power-distribution criterion is acceptable.

[3]This simplification is feasible, because the dynamics model is built for actuation-mode optimization rather than for control.

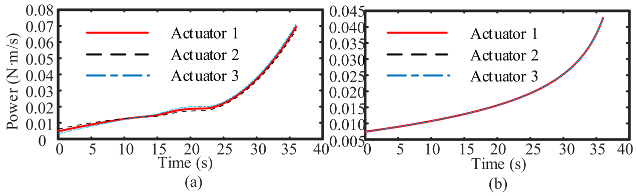

Fig. 17. Experimental and theoretical results under folding mode.

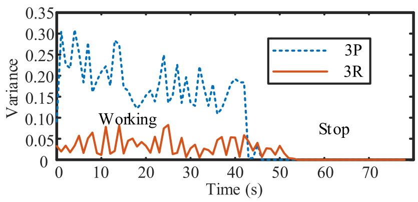

Fig. 18. Experimental variance under the power-requirement criterion: two distinct actuation modes.

C. Verification of the Actuation-Mode Analysis

In this section, the properties of the 3R and 3P actuation modes are directly compared by experiments.

1) The Test Based on Actuation-Strategy Criterion: It is found, from the maneuvers in Fig. 13, that only one actuator of the 3P-type works, and three for the 3R-type under the bending mode. Thus, the 3P-type prototype is suitable for the bending task. In turn, three actuators of the 3R-type are required to work together with high precision fit and reasonable trajectory planning. In this case, therefore, the 3P actuation mode is optimum, which matches the theoretical analysis in Sections V-D and V-E.

2) The Test Based on The Power-Distribution Criterion: Our prototypes are designed for a multiple-modular manipulator, whereby the 3R- and 3P-type modules have different reachable workspaces for various roles in the system. Therefore, the experiment here is an approximate verification. Fig. 18 represents the experimental variance of three actuators in the 3R- and 3P-type modes, under the bending motion. The figure shows that the variance of the 3R-type is smaller than that of the 3P-type. Therefore, the 3R-type shows a more even distribution of power requirements, thereby being the optimal solution. This matches the analysis in Sections V-C and V-E.

VIII. Conclusion

The authors proposed a method for the analysis of the actuation modes of multiloop mechanisms for space applications. Three basic evaluation criteria, namely, actuator generalized-force distribution, power requirement, and actuation strategy, were established. With these criteria, we just chose the desired mode among the elements of a discrete set. Thus, a rather complex problem is solved in a simple manner. The method is then used to select the actuation-mode applicable to the DTMLM. By means of the power-requirement model, the optimum modes of the DTMLM under different viewpoints are obtained. The 3R-type shows an even power-consumption distribution among the three actuators. By contrast, in the 3P-type, one single actuator is operational, and hence, takes all the load.

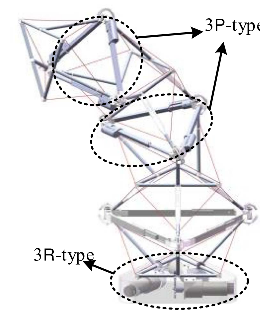

Fig. 19. A three-module space manipulator with two distinct types of actuation modes.

When an N-modular DTMLM manipulator is applied for space capturing, $3N$ actuators are needed to drive the system. In this case, the actuation-strategy criterion leads to the simplest actuation mode. Thus, a comprehensive application of the 3R-, 3P-, 2R1P-, and 1R2P- actuation modes is suitable to control a multimodular manipulator of the class described here. Shown in Fig. 19 is a manipulator with three modules. The first module, the one closest to the BP, applies a 3R actuation mode for a good power output, whereas the second and the third modules require a 3P actuation mode for the simplest actuation strategy. In this case, only five, instead of nine, actuators are operational for a bending action, thereby being suitable for capturing or reconfiguration tasks.

Moreover, since the DTMLM operates under special conditions, such as a zero-gravity environment, a number of full actuation-mode possibilities and multiloop configurations are available. Furthermore, for mechanical systems with actuation modes under which gravity plays a minor role, such as a) robots under low-speed uniform maneuvers and b) robots with light actuators, our actuation strategy should be effective for the optimum selection of the actuation mode(s).

Further to the work reported here, actuation robustness, reliability, and resilience [5], [31] will be investigated, along with dynamics and control strategies.

Appendix

1) Link 13: From the actuated and constraint Jacobian matrices of the DTMLM in our early work [2], $\boldsymbol{\omega}_{13} = \mathbf{K}\dot{\mathbf{c}}_{13}$ and $\dot{\mathbf{c}}_{13} = \mathbf{B}\dot{\mathbf{q}}$ are derived, where $\mathbf{K}$ and $\mathbf{B}$ are 3×3 matrices. We thus have

$\mathbf{t}_{13,i} = \begin{bmatrix} \mathbf{w}_{13,i}^T & \mathbf{v}_{13,i}^T \end{bmatrix}^T$, where $\mathbf{w}_{13,i}$ and $\mathbf{v}_{13,i}$ represent the ith column vector in $\mathbf{KB}$ and $\mathbf{B}$, respectively.

2) Links 1–3: If $\mathbf{a}_i$ represents the unit vector of $\overrightarrow{A_iB_i}$, then $\mathbf{t}_{11} = \begin{bmatrix} \mathbf{e}_1 \\ l/2(\mathbf{e}_1 \times \mathbf{a}_1) \end{bmatrix}$, $\mathbf{t}_{22} = \begin{bmatrix} \mathbf{e}_2 \\ l/2(\mathbf{e}_2 \times \mathbf{a}_2) \end{bmatrix}$, $\mathbf{t}_{33} = \begin{bmatrix} \mathbf{e}_3 \\ l/2(\mathbf{e}_3 \times \mathbf{a}_3) \end{bmatrix}$.

3) Links 4–9: Let $\mathbf{n}_{12}$, $\mathbf{n}_{23}$, and $\mathbf{n}_{31}$ represent the unit vector of $\overrightarrow{B_1B_2}$, $\overrightarrow{B_2B_3}$, and $\overrightarrow{B_3B_1}$, respectively, l_j the length of the jth link.

$$\mathbf{t}_{4,i} = \begin{bmatrix} \mathbf{w}_{4,i}^T & \mathbf{v}_{4,i}^T \end{bmatrix}^T, \text{ where}$$
$$\mathbf{w}_{41} = (\mathbf{w}_{13,1}^T \mathbf{n}_{12})\mathbf{n}_{12}/2 + \mathbf{b}_{12} \times (l\mathbf{e}_1 \times \mathbf{a}_1)/\|\mathbf{b}_{12}\|^2$$
$$\mathbf{w}_{42} = (\mathbf{w}_{13,2}^T \mathbf{n}_{12})\mathbf{n}_{12}/2 - \mathbf{b}_{12} \times (l\mathbf{e}_2 \times \mathbf{a}_2)/\|\mathbf{b}_{12}\|^2$$
$$\mathbf{w}_{43} = (\mathbf{w}_{13,3}^T \mathbf{n}_{12})\mathbf{n}_{12}/2, \mathbf{v}_{41} = l\mathbf{e}_1 \times \mathbf{a}_1 + l_4\mathbf{w}_{41}/2 \times \mathbf{n}_{12}$$
$$\mathbf{v}_{42} = l_4\mathbf{w}_{42}/2 \times \mathbf{n}_{12}, \mathbf{v}_{43} = l_4\mathbf{w}_{43}/2 \times \mathbf{n}_{12}$$
$$\mathbf{t}_{5,i} = \begin{bmatrix} \mathbf{w}_{5,i}^T & \mathbf{v}_{5,i}^T \end{bmatrix}^T, \text{ where}$$
$$\mathbf{w}_{51} = \mathbf{w}_{41}, \mathbf{w}_{52} = \mathbf{w}_{42}, \mathbf{w}_{53} = \mathbf{w}_{43}$$
$$\mathbf{v}_{51} = -l_5\mathbf{w}_{51} \times \mathbf{n}_{12}/2, \mathbf{v}_{52} = l\mathbf{e}_2 \times \mathbf{a}_2 - l_5\mathbf{w}_{52} \times \mathbf{n}_{12}/2$$
$$\mathbf{v}_{53} = -l_5\mathbf{w}_{53} \times \mathbf{n}_{12}/2$$
$$\mathbf{t}_{6,i} = \begin{bmatrix} \mathbf{w}_{6,i}^T & \mathbf{v}_{6,i}^T \end{bmatrix}^T, \text{ where}$$
$$\mathbf{w}_{62} = (\mathbf{w}_{13,2}^T \mathbf{n}_{23})\mathbf{n}_{23}/2 + \mathbf{b}_{23} \times (l\mathbf{e}_2 \times \mathbf{a}_2)/\|\mathbf{b}_{23}\|^2$$
$$\mathbf{w}_{63} = (\mathbf{w}_{13,3}^T \mathbf{n}_{23})\mathbf{n}_{23}/2 - \mathbf{b}_{23} \times (l\mathbf{e}_3 \times \mathbf{a}_3)/\|\mathbf{b}_{23}\|^2$$
$$\mathbf{w}_{61} = (\mathbf{w}_{13,1}^T \mathbf{n}_{23})\mathbf{n}_{23}/2, \mathbf{v}_{62} = l\mathbf{e}_2 \times \mathbf{a}_2 + l_6\mathbf{w}_{62} \times \mathbf{n}_{23}/2$$
$$\mathbf{v}_{63} = l_6\mathbf{w}_{63} \times \mathbf{n}_{23}/2, \mathbf{v}_{61} = l_6\mathbf{w}_{61} \times \mathbf{n}_{23}/2$$
$$\mathbf{t}_{7,i} = \begin{bmatrix} \mathbf{w}_{7,i}^T & \mathbf{v}_{7,i}^T \end{bmatrix}^T, \text{ where}$$
$$\mathbf{w}_{72} = \mathbf{w}_{62}, \mathbf{w}_{73} = \mathbf{w}_{63}, \mathbf{w}_{71} = \mathbf{w}_{61}$$
$$\mathbf{v}_{72} = -l_7\mathbf{w}_{72} \times \mathbf{n}_{23}, \mathbf{v}_{73} = l\mathbf{e}_3 \times \mathbf{a}_3 - l_7\mathbf{w}_{73} \times \mathbf{n}_{23}/2$$
$$\mathbf{v}_{71} = -l_7\mathbf{w}_{71} \times \mathbf{n}_{23}/2$$
$$\mathbf{t}_{8,i} = \begin{bmatrix} \mathbf{w}_{8,i}^T & \mathbf{v}_{8,i}^T \end{bmatrix}^T, \text{ where}$$
$$\mathbf{w}_{83} = (\mathbf{w}_{13,3}^T \mathbf{n}_{31})\mathbf{n}_{31}/2 + \mathbf{b}_{31} \times (l\mathbf{e}_3 \times \mathbf{a}_3)/\|\mathbf{b}_{31}\|^2$$
$$\mathbf{w}_{81} = (\mathbf{w}_{13,1}^T \mathbf{n}_{31})\mathbf{n}_{31}/2 - \mathbf{b}_{31} \times (l\mathbf{e}_1 \times \mathbf{a}_1)/\|\mathbf{b}_{31}\|^2$$
$$\mathbf{w}_{82} = (\mathbf{w}_{13,2}^T \mathbf{n}_{31})\mathbf{n}_{31}/2, \mathbf{v}_{83} = l\mathbf{e}_3 \times \mathbf{a}_3 + l_8\mathbf{w}_{83} \times \mathbf{n}_{31}/2$$
$$\mathbf{v}_{81} = l_8\mathbf{w}_{81} \times \mathbf{n}_{31}/2, \mathbf{v}_{82} = l_8\mathbf{w}_{82} \times \mathbf{n}_{31}/2$$
$$\mathbf{t}_{9,i} = \begin{bmatrix} \mathbf{w}_{9,i}^T & \mathbf{v}_{9,i}^T \end{bmatrix}^T, \text{ where}$$
$$\mathbf{w}_{93} = \mathbf{w}_{83}, \mathbf{w}_{91} = \mathbf{w}_{81}, \mathbf{w}_{92} = \mathbf{w}_{82}$$
$$\mathbf{v}_{93} = -l_9\mathbf{w}_{93} \times \mathbf{n}_{31}/2, \mathbf{v}_{91} = l\mathbf{e}_1 \times \mathbf{a}_1 - l_9\mathbf{w}_{91} \times \mathbf{n}_{31}/2$$
$$\mathbf{v}_{92} = -l_9\mathbf{w}_{92} \times \mathbf{n}_{31}/2.$$

4) Links 10–12: Let $\mathbf{a}_{10}$, $\mathbf{a}_{11}$, and $\mathbf{a}_{12}$ represent the unit vectors of $\overrightarrow{B_1D_1}$, $\overrightarrow{B_2D_2}$, and $\overrightarrow{B_3D_3}$, respectively.

$$\mathbf{t}_{10,i} = \begin{bmatrix} \mathbf{w}_{10,i}^T & \mathbf{v}_{10,i}^T \end{bmatrix}^T, \text{ where}$$
$$\mathbf{w}_{10,1} = \mathbf{w}_{13,1} + \mathbf{e}_{10}, \mathbf{w}_{10,2} = \mathbf{w}_{13,2}, \mathbf{w}_{10,3} = \mathbf{w}_{13,3}$$
$$\mathbf{v}_{10,1} = l\mathbf{e}_1 \times \mathbf{a}_1 + l\mathbf{w}_{10,1} \times \mathbf{a}_{10}/2$$
$$\mathbf{v}_{10,2} = l\mathbf{w}_{10,2} \times \mathbf{a}_{10}/2, \mathbf{v}_{10,3} = l\mathbf{w}_{10,3} \times \mathbf{a}_{10}/2$$
$$\mathbf{t}_{11,i} = \begin{bmatrix} \mathbf{w}_{11,i}^T & \mathbf{v}_{11,i}^T \end{bmatrix}^T, \text{ where}$$
$$\mathbf{w}_{11,1} = \mathbf{w}_{13,1}, \mathbf{w}_{11,2} = \mathbf{w}_{13,2} + \mathbf{e}_{11}, \mathbf{w}_{11,3} = \mathbf{w}_{13,3}$$
$$\mathbf{v}_{11,1} = l\mathbf{w}_{11,1} \times \mathbf{a}_{11}/2, \mathbf{v}_{11,2} = l\mathbf{e}_2 \times \mathbf{a}_2 + l\mathbf{w}_{11,2} \times \mathbf{a}_{11}/2$$
$$\mathbf{v}_{11,3} = l\mathbf{w}_{11,3} \times \mathbf{a}_{11}/2$$
$$\mathbf{t}_{12,i} = \begin{bmatrix} \mathbf{w}_{12,i}^T & \mathbf{v}_{12,i}^T \end{bmatrix}^T, \text{ where}$$
$$\mathbf{w}_{12,1} = \mathbf{w}_{13,1}, \mathbf{w}_{12,2} = \mathbf{w}_{13,2}, \mathbf{w}_{12,3} = \mathbf{w}_{13,3} + \mathbf{e}_{12}$$
$$\mathbf{v}_{12,1} = l\mathbf{w}_{12,1} \times \mathbf{a}_{12}/2, \mathbf{v}_{12,2} = l\mathbf{w}_{12,2} \times \mathbf{a}_{12}/2$$
$$\mathbf{v}_{12,3} = l\mathbf{e}_3 \times \mathbf{a}_3 + l\mathbf{w}_{12,3} \times \mathbf{a}_{12}/2.$$

REFERENCES

[1] C. Li, H. Guo, D. Tang, H. Yan, R. Liu, and Z. Deng, "A 3-R(SRS)RP multi-loop mechanism for space manipulation: Design, kinematics, singularity, and workspace," *ASME Tans. J. Mechanisms Robot.*, vol. 12, no. 1, 2020, Art. no. 011001.

[2] C. Li *et al.*, "Mobility and singularity analyses of a symmetric multi-loop mechanism for space applications," *Proc. IMechE Part C: J. Mech. Eng. Sci.*, early access, 2021, doi: 10.1177/0954406221995555.

[3] T. Laliberté, L. Birglen, and C. Gosselin, "Underactuation in robotic grasping hands," *Mach. Intell. Robot. Control*, vol. 4, no. 3, pp. 1–11, 2002.

[4] L. Birglen, T. Laliberté, and C. M. Gosselin, *Underactuated Robotic Hands*. Berlin, Germany: Springer, 2007, vol. 40.

[5] T. Zhang, W. Zhang, and M. M. Gupta, "An underactuated self-reconfigurable robot and the reconfiguration evolution," *Mechanism Mach. Theory*, vol. 124, pp. 248–258, 2018.

[6] D. Liang, Y. Song, T. Sun, and G. Dong, "Optimum design of a novel redundantly actuated parallel manipulator with multiple actuation modes for high kinematic and dynamic performance," *Nonlinear Dyn.*, vol. 83, nos. 1–2, pp. 631–658, 2016.

[7] C. Cheng, W. Xu, and J. Shang, "Optimal distribution of the actuating torques for a redundantly actuated masticatory robot with two higher kinematic pairs," *Nonlinear Dyn.*, vol. 79, no. 2, pp. 1235–1255, 2015.

[8] B.-J. Yi, S.-R. Oh, and I. H. Suh, "A five-bar finger mechanism involving redundant actuators: Analysis and its applications," *IEEE Trans. Robot. Automat.*, vol. 15, no. 6, pp. 1001–1010, Dec. 1999.

[9] J. H. Choi, T. Seo, and J. W. Lee, "Torque distribution optimization of redundantly actuated planar parallel mechanisms based on a null-space solution," *Robotica*, vol. 32, no. 7, 2014, Art. no. 1125.

[10] J. Hollerbach and K. Suh, "Redundancy resolution of manipulators through torque optimization," *IEEE J. Robot. Autom.*, vol. 3, no. 4, pp. 308–316, Aug. 1987.

[11] N. Mostashiri, J. Dhupia, A. Verl, J. Bronlund, and W. Xu, "Optimizing the torque distribution of a redundantly actuated parallel robot to study the temporomandibular reaction forces during food chewing," *J. Mechanisms Robot.*, vol. 12, no. 5, 2020, Art. no. 051008.

[12] Y. Zhang and J. Wang, "A dual neural network for constrained joint torque optimization of kinematically redundant manipulators," *IEEE Trans. Syst., Man, Cybern., Part B. (Cybern.)*, vol. 32, no. 5, pp. 654–662, Oct. 2002.

[13] J. Yao, W. Gu, Z. Feng, L. Chen, Y. Xu, and Y. Zhao, "Dynamic analysis and driving force optimization of a 5-DOF parallel manipulator with redundant actuation," *Robot. Comput.- Integr. Manuf.*, vol. 48, pp. 51–58, 2017.

[14] W. Xu, H. Chen, H. Zhao, and B. Ren, "Torque optimization control for electric vehicles with four in-wheel motors equipped with regenerative braking system," *Mechatronics*, vol. 57, pp. 95–108, 2019.

[15] W. Jia, G. Yang, C. Wang, C. Zhang, C. Chen, and Z. Fang, "Energy-efficient torque distribution optimization for an omnidirectional mobile robot with powered caster wheels," *Energies*, vol. 12, no. 23, 2019, Art. no. 4417.

[16] R. Ur-Rehman, S. Caro, D. Chablat, and P. Wenger, "Multi-objective path placement optimization of parallel kinematics machines based on energy consumption, shaking forces and maximum actuator torques: Application to the orthoglide," *Mechanism Mach. Theory*, vol. 45, no. 8, pp. 1125–1141, 2010.

[17] S. Kucuk, "Energy minimization for 3-RRR fully planar parallel manipulator using particle swarm optimization," *Mechanism Mach. Theory*, vol. 62, pp. 129–149, 2013.

[18] Y. Li *et al.*, "Optimization of dynamic load distribution of a serial-parallel hybrid humanoid arm," *Mechanism Mach. Theory*, vol. 149, 2020, Art. no. 103792.

[19] W. Zhao and R. K. Kapania, "Actuator energy and drag minimization of a blended-wing-body with variable-camber continuous trailing-edge flaps," *Eng. Optim.*, vol. 52, no. 9, pp. 1561–1587, 2020.

[20] D. Schwung, T. Kempe, A. Schwung, and S. X. Ding, "Self-optimization of energy consumption in complex bulk good processes using reinforcement learning," in *Proc. IEEE 15th Int. Conf. Ind. Inform.*, 2017, pp. 231–236.

[21] M. Hassan and A. Khajepour, "Optimization of actuator forces in cable-based parallel manipulators using convex analysis," *IEEE Trans. Robot.*, vol. 24, no. 3, pp. 736–740, Jun. 2008.

[22] B.-T. Wang, R. A. Burdisso, and C. R. Fuller, "Optimal placement of piezoelectric actuators for active structural acoustic control," *J. Intell. Mater. Syst. Struct.*, vol. 5, no. 1, pp. 67–77, 1994.

[23] F. Mu, X. Zhongmin, and T. Hornsen, "Distributed multi-flexoelectric actuation and control of plates," *AIAA J.*, vol. 58, no. 3, pp. 1377–1385, 2020.

[24] Y. J. Shin and K.-S. Kim, "Distributed-actuation mechanism for a finger-type manipulator: Theory and experiments," *IEEE Trans. Robot.*, vol. 26, no. 3, pp. 569–575, Jun. 2010.

[25] E. A. B. Nieto, S. Rezazadeh, and R. D. Gregg, "Minimizing energy consumption and peak power of series elastic actuators: A convex optimization framework for elastic element design," *IEEE/ASME Trans. Mechatronics*, vol. 24, no. 3, pp. 1334–1345, Jun. 2019.

[26] T. Lagger, P. Smith, M. Kuczaj, and R. Romana, “Geared rotary power distribution unit with mechanical differential gearing for multiple actuator systems,” U.S. Patent App. 16/143,335, Mar. 26, 2020 .

[27] C. Zhao, H. Guo, R. Liu, Z. Deng, B. Li, and J. Tian, “Actuation distribution and workspace analysis of a novel 3 (3RRLS) metamorphic serial-parallel manipulator for grasping space non-cooperative targets,” *Mechanism Mach. Theory*, vol. 139, pp. 424–442, 2019.

[28] X. Ding, H. Xiao, Q. Yang, L. Li, and K. Xu, “Design and analysis of a cable-winding device driving large deployable mechanisms in astrophysics missions,” *Acta Astronautica*, vol. 169, pp. 124–137, 2020.

[29] H. Xiao, S. Liu, and X. Ding, “Optimizing accuracy of a parabolic cylindrical deployable antenna mechanism based on stiffness analysis,” *Chin. J. Aeronaut.*, vol. 33, no. 170(05), pp. 192–202, 2020.

[30] C. Li *et al.*, “Cell division method for mobility analysis of multi-loop mechanisms,” *Mechanism Mach. Theory*, vol. 141, pp. 67–94, 2019.

[31] W. Zhang and C. Van Luttervelt, “Toward a resilient manufacturing system,” *CIRP Ann.*, vol. 60, no. 1, pp. 469–472, 2011.

Chuanyang Li received the M.S. and Ph.D. degrees in mechanical engineering from the Harbin Institute of Technology, Harbin, China, in 2016 and 2021, respectively. He was a Visiting Ph.D. Student from 2019 to 2020 with McGill University, supervised by Prof. Jorge Angeles.

He is currently a Lecturer with the Department of Basic, PLA Rocket Force University of Engineering, Xi’an, China. His research interests include multiloop mechanisms, space manipulators, and space capture.

Jorge Angeles (Life Fellow, IEEE) received the Engineering Diploma in electromechanical engineering and the M.Eng. degree in mechanical engineering from Universidad Nacional Autónoma de México (UNAM), Mexico City, Mexico, in 1969 and 1970, respectively, and the Ph.D. degree in applied mechanics from Stanford University, Stanford, CA, USA, in 1973.

Since 1984, he has been with the Department of Mechanical Engineering, McGill University, Montreal, QC, Canada, and became a Founding Member of the Centre for Intelligent Machines, in 1985, where he is currently a Professor Emeritus of Mechanical Engineering. He was with the Faculty of the Department of Mechanical Engineering, UNAM, for 11 years.

Dr. Angeles is one of the 12 honorary members of IFToMM and fellow of The Royal Society of Canada, the Canadian Society for Mechanical Engineering, ASME, IEEE, and the Canadian Academy of Engineering.

Hongwei Guo received the M.S. and Ph.D. degrees in mechanical engineering from the Harbin Institute of Technology, Harbin, China, in 2005 and 2009, respectively.

He is currently a Professor with the School of Mechatronics Engineering, Harbin Institute of Technology. Since 2020, he has been involved in Young Changjiang Scholars Programme of China. He has authored and co-authored more than 80 articles and holds more than 40 patents. His research interests include space-folding mechanisms and deformed wings.

Dewei Tang received the M.S. and Ph.D. degrees in mechanical engineering from the Harbin Institute of Technology, Harbin, China, in 1991 and 2000, respectively.

Since 2005, he has been a Professor with the School of Mechatronics Engineering, Harbin Institute of Technology. He has authored and coauthored more than 110 articles and holds 25 patents. Since 2010, he has been participating in the third phase project of the Chinese lunar exploration. His research interests include drilling performance analysis and enhancement in extreme environments and undisturbed sampling techniques.

Rongqiang Liu received the M.S. and Ph.D. degrees in mechanical engineering from the Harbin Institute of Technology, Harbin, China, in 1989 and 1995, respectively.

Since 2004, he has been a Professor with the School of Mechatronics Engineering, Harbin Institute of Technology. He has authored and co-authored more than 80 articles and holds more than 10 patents. He has been involved in more than 10 projects such as the National Natural Science Foundation of China and the “863” project. His research interests include space-folding mechanisms, adaptive structures, mechanical design, kinematics, and dynamics and control.

Zhongbao Qin received the M.S. and Ph.D. degrees in mechanical engineering from Northwestern Polytechnical University, Xi’an, China, in 2001 and 2006, respectively.

He is currently an Associate Professor with the Department of Basic, PLA Rocket Force University of Engineering, Xia’n, China. His research interests include inspection, monitoring, and fault diagnosis of special machinery equipment.

Hong Xiao received M.S. and Ph.D. degrees in mechanical engineering from the Harbin Institute of Technology, Harbin, China, in 2013 and 2018, respectively.

He is currently a Postdoctoral Researcher with the Harbin Institute of Technology (Shenzhen), Shenzhen, China. His research interests include thermal analysis, dynamic analysis of transmission systems, adaptive structure, and capturing.